

Application of the adsorbent CR-100 for Ammonium Removal: Thermodynamic and Kinetic Studies

Arpad Kiralj,¹ Željko Tomić,² Milica Hadnadjev-Kostic,^{1,*} Nataša Lukić,¹ Tatjana Vulić,¹
 Jovana Grahovac,¹ Aleksandar Jokić¹

¹ University of Novi Sad, Faculty of Technology Novi Sad, Bulevar cara Lazara 1, Novi Sad, Serbia

² Institute for Work Safety, Marka Miljanova 9-9A, Novi Sad, Serbia

* Corresponding author's e-mail address: hadnadjev@tf.uns.ac.rs

RECEIVED: October 12, 2021 * REVISED: April 19, 2022 * ACCEPTED: May 2, 2022

Abstract: Groundwater with increased ammonia concentration is a constant concern regarding the preparation of drinking water. The affinity of ammonia to be adsorbed on the surface of different solid materials significantly influences the selection of its removal process and has been the motivation for this investigation. Crystal-Right™ (CR-100) was used for the removal of ammonia from aqueous solution in batch adsorption procedure. The kinetics of adsorption followed the pseudo-second-order model. The Elovich model suggested that chemisorption rate decreased with the temperature increase. The liquid film diffusion and intra-particle diffusion models revealed that heterogeneous adsorbent surface energy had a particularly pronounced impact on the overall mass transfer rate. The Arrhenius and Eyring's equations suggested spontaneous and endothermic nature of complex adsorption/ion exchange removal process. The isosteric heat of adsorption revealed that with the increase in surface loading lateral interactions between the adsorbed molecules occurred.

Keywords: groundwater treatment, synthetic mesoporous adsorbent, adsorption, isosteric heat of adsorption.

INTRODUCTION

GROUNDWATER with increased ammonia concentration containing humic substances is a frequent occurrence in Vojvodina, Northern Serbia. Arsenic, borates, natural organic substances, ammonia, iron, sodium and manganese can be identified in water samples at different locations^[1,2] with concentrations above the permitted values.^[3] In terms of drinking water quality, endangered areas in Vojvodina, Northern Serbia are the southwestern parts of Backa, as well as areas of central and northern Banat due to the lack of adequate facilities for the preparation of drinking water in these regions. The identified organic substances, such as ammonia, in the groundwater of Vojvodina originate from water pollution due to anthropogenic factors, such as the influence of industry or agricultural activities, as well as from nature depending on the of groundwater source.^[3] The preparation of drinking water from waters that contain

ammonia is problematic regarding the procedure for the removal of this pollutant. Previous processes that have been applied are based on microbiological activities, chemical oxidation, membrane technologies, adsorption and many other procedures.^[4–7]

The affinity of ammonia to adsorb on the surface of different solid materials significantly influences the selection of its removal process.^[8–10] There are various adsorbent materials in nature that are successfully applied for this purpose,^[11–14] such as zeolites,^[15–21] clay minerals, activated carbon, exfoliated vermiculites, fly ash, peats, chitosan beads, wood sawdust, bentonite, attapulgite, oxide nanoparticles, and zero-valent iron that have ion exchange and adsorption properties.^[22–28]

Crystal-Right™ (CR-100) is one of the most durable synthetic mesoporous aluminosilicate used for commercial purposes^[29] and has the ability to increase the pH value, to reduce water hardness and remove iron and manganese ions^[30] during the filtration process. Furthermore together

with these desired properties, adsorbent CR-100 can easily be regenerated after the rinsing (washing) process.

Water supply in the region of northern Banat in Vojvodina, Northern Serbia is mainly based on springs that exploit groundwater with water quality parameter values above maximum permitted amounts (MPA) according to Regulations on hygienic correctness of drinking water published in Official gazette („Službeni list SRJ“, br. 42/98 i 44/99). For example, analysed groundwater from wells in municipality of Kikinda has ammonium ion amount of 2.07 mg L⁻¹ which exceeds 20 times higher than the ammonium ion MPA (0.1 mg L⁻¹).^[31] Considering the permanent need to supply high quality drinking water in this Serbian region, the aim of this study was to investigate the possibility of CR-100 adsorbent application for the removal of ammonium ions from water solutions. In order to elucidate kinetics and thermodynamics of adsorption process, the influence of adsorbent-adsorbate contact time and temperature on the efficiency of the adsorption was studied. Additionally, for the understanding of the process dynamics that can be applied for the development of adsorbents on an industrial level, different mathematical models for the adsorption process were considered.

EXPERIMENTAL

The study of the adsorption was carried out on the laboratory scale using mesoporous aluminosilicate as the adsorbent and ammonia model solution as adsorbate. Ammonium chloride (concentration of 3 mg NH₄⁺-N L⁻¹ - ammonium ion (NH₄⁺)-nitrogen (N) in the litre of ultra-pure water), prepared by dissolving solid NH₄Cl (Sigma-Aldrich, p.a.) in ultra-pure water, was used as model solution.

Adsorbent Characterization

Crystal Right™ (type CR-100) was characterized by chemical and textural analysis. The chemical composition of adsorbents was determined by atomic adsorption spectrophotometry. The textural characterization, specific surface area and the pore size distribution were conducted by low-temperature nitrogen adsorption at -196 °C, on Micromeritics ASAP 2000. The specific surface area was calculated by the multipoint Brunauer-Emmer-Teller (BET) method, whereas the pore size distribution was determined using Brunauer-Joyner-Hallenda (BJH) method and the desorption branch of the isotherm. Prior to textural analysis, the samples were degassed at 150 °C for 12h in order to remove any impurities from the adsorbent surface. The adsorption process was estimated based on the adsorption isotherms. Experimental data of the adsorption process exhibited the best fit for the Freundlich adsorption isotherm.^[32,33]

$$\log(q_t) = \log(K_f) + \frac{1}{n} \cdot \log(C) \quad (1)$$

where q_t (mg g⁻¹) is the adsorption capacity at equilibrium conditions; C (mg L⁻¹) – equilibrium concentration of adsorbates in solution, K_f – parameter related to the binding capacity of the adsorbate and $1/n$ – constant indicating the adsorbent affinity for the adsorbate.

Batch Adsorption Procedure

The adsorbent sample was measured using analytical balance (Precisa, Switzerland, type XT 220 A) and dried for 2h at 180 °C (Vims electronic, Serbia, type LSW-53 furnace). After drying sample was cooled and weighted in order to determine the moisture percentage (4.14 % ± 2 %). The sample was washed with ultra-pure water (UPW), filtered (LLG-qualitative, slow filter paper) to remove fine particles and dried. Closed 250 ml ground neck flasks with 100 ml of ammonium-chloride solution and adsorbent sample were placed on Thermo Scientific, USA, type Ploy 15 apparatus with magnetic stirrers, located in the thermostatic device. Tests at three different temperatures (279, 289 and 299 K) were performed. The adsorbent-adsorbate contact time was 120 minutes. The amount of adsorbed ammonia was measured at following time intervals: 10, 20, 30, 60, 90 and 120 minutes. The solution from the flasks was decanted and filtered through a 0.22 μm syringe filter (Nylon Syringe filter - AMTAST). Ion chromatography was used to determine the concentrations of ammonia, sodium, potassium, calcium and magnesium in the solution after the adsorption (Dionex Corporation USA, type IC / ICS 3000). Kinetic tests were performed with adsorbent concentration of 0.08 g L⁻¹. All experiments were conducted in triplicates and the mean value was used for all presented calculations.

Adsorption Kinetic Models

In order to investigate the adsorption kinetics, the adsorption capacity at equilibrium conditions was calculated using the following equation:

$$q_e = \frac{C_0 - C_e}{m} \cdot V \quad (2)$$

where q_e (mg g⁻¹) was adsorption capacity at equilibrium conditions, C_0 was the initial concentration (mg NH₄⁺-N L⁻¹), C_e was the equilibrium concentration of ammonia in the solution (mg NH₄⁺-N L⁻¹), V was the volume of the ammonia-chloride (L) and m is the adsorbent mass (mg).

The adsorption rate was determined in correlation with the adsorbed ammonia amount at different adsorbent-adsorbate contact time using different models.^[34–36] For the pseudo-first order (PFO) and pseudo-second order (PSO) kinetics the following equations were used:

$$\ln(q_e - q_t) = \ln q_e - k_1 \cdot t \quad (3)$$

$$\frac{t}{q_t} = \frac{1}{k_2 q_e} + \frac{1}{q_e} \cdot t \quad (4)$$

where q_e (mg g⁻¹) was adsorption capacity at equilibrium conditions; q_t (mg g⁻¹) adsorption capacity at the defined time t (min), k_1 (mg g⁻¹min⁻¹) rate constant for the pseudo first-order model and k_2 (g mg⁻¹min⁻¹) rate constant for the pseudo second-order model. Initial adsorption rate can also be estimated from the reciprocal value of the model ordinate section, h :

$$h = k_2 q_e^2 \quad (5)$$

For the determination of the adsorption limiting step the following kinetic models were applied: Elovich model (Eq. 6), liquid film diffusion (Eq. 7) and intra-particle diffusion model (Eq. 8):

$$q_t = \beta \cdot \ln(\alpha \cdot \beta) + \beta \cdot \ln(t) \quad (6)$$

$$\ln(1 - F) = -k_{fd} \cdot t \quad (7)$$

$$q_t = k_i \cdot t^{1/2} \quad (8)$$

where α (mg g⁻¹ min⁻¹) was initial adsorption rate, β (g mg⁻¹) desorption constant, F (ratio q_t/q_e) fractional attainment of equilibrium, k_{fd} (min⁻¹) rate constant of mass transfer through the liquid film and k_i (mg g⁻¹ min^{-1/2}) intra-particle diffusion (IPD) rate constant. The suitability of these models is assessed by R^2 values that are close to unity. Adsorption kinetic data can be modelled using linear or non-linear regression methods. The two regression methods also yielded significantly different values of model parameters. The drawback of model linearization can be detected when the model predictions are plotted with the experimental data in the non-linear form (i.e. as the adsorbed amount vs. time).^[32] In this study for the adsorption kinetic modelling linear and non-linear regression methods were used for PFO, PSO and Elovich models.

Thermodynamics of Ammonia Adsorption

For the pseudo second-order model, the reaction rate constant, k_2 , at the selected temperatures (279 K, 289 K, and 299 K) was used to calculate the activation thermodynamic parameters of the observed adsorption process. The activation energy of ammonia adsorption on the adsorbent was calculated using the Arrhenius equation:

$$\ln k_2 = \ln A - \frac{E_a}{R \cdot T} \quad (9)$$

where E_a (kJ mol⁻¹) was the activation energy, A Arrhenius pre-exponential factor, R universal gas constant ($R = 8.314$ J mol⁻¹ K⁻¹), T temperature (K) and k_2 rate constant of the pseudo second-order (g mg⁻¹ min⁻¹).

Another expression used to describe the dependence of the pseudo second-order constant reaction rate and temperature was the Eyring's equation:

$$\ln\left(\frac{k_2}{T}\right) = \left(\ln\left(\frac{k_B}{T}\right) + \frac{\Delta S^*}{R}\right) + \frac{\Delta H^*}{RT} \quad (10)$$

where ΔH^* (kJ mol⁻¹) was activation enthalpy, ΔS^* (kJ mol⁻¹ K⁻¹) activation entropy, k_B Boltzmann's constant ($k_B = 1.38 \times 10^{-23}$ J K⁻¹) and h Planck's constant ($h = 6.63 \times 10^{-34}$ J s).

The spontaneity of the adsorption process was determined based on the change in the standard free Gibbs energy, ΔG , by the following expressions:

$$\Delta G = \Delta H - T\Delta S \quad (11)$$

$$\Delta G = -RT \ln K_c \quad (12)$$

where ΔG (J mol⁻¹) was change in the standard free Gibbs energy and K_c thermodynamic equilibrium constant.

Thermodynamic equilibrium constant was determined from the Khan and Singh procedure^[37] and the thermodynamic equilibrium constant was calculated from the $\ln(q_e/C_e) - q_e$, dependence based on the adsorption isotherm equilibrium data. The value of the equilibrium constant was obtained by extrapolation to $q_e = 0$. Taking into account the Milonjić correction,^[37] the constant was multiplied by 1000 (1 dm³ = 1000 ml (or g, since the solution density is ≈ 1 g ml⁻¹)) in order to obtain a dimensionless value.

Isotheric heat can be used to determine the adsorption type as well as to characterize the adsorbent surface, necessary for the design of both the adsorption process and the equipment for the adsorption process. Isotheric heat can be defined as the heat generated during the adsorption of adsorbate unit amount (1 mol) at its constant concentration on the adsorbent surface.^[36] The isotheric heat of adsorption was calculated from the Claussius-Clapeyron equations:

$$\frac{d \ln C_e}{dT} = \frac{-\Delta H_{st,a}}{RT^2} \quad (13)$$

$$\Delta H_{st,a} = R \frac{d \ln C_e}{d(1/T)} \Big|_{q_e} \quad (14)$$

where C_e was equilibrium concentration in solution at a constant amount of adsorbed cation obtained from adsorption isotherm data and $\Delta H_{st,a}$ isotheric heat.

RESULTS AND DISCUSSION

In accordance with the previously published study,^[29] chemical analysis of the adsorbent Crystal Right™ (type CR-100) confirmed predominant presence of Si, Al, and O,

Table 1. Chemical analysis of component amount for the aluminosilicate adsorbent CR-100.

Si(%)	O(%)	Al(%)	Na(%)	K(%)	Ca(%)	Mg(%)	Mg(%)
51.6	33.915	7.28	6.54	0.17	0.34	0.14	0.015

as well as the presence of Na, K, Ca and Mg as adsorbent extra framework cations with Fe impurities, Table 1. Textural analysis revealed that the adsorption-desorption isotherm corresponded to type IVa characteristic for mesoporous materials such as industrial adsorbents, oxide gels and mesoporous molecular sieves, whereas the hysteresis loop corresponded to type H1 typical for materials with a narrow range of uniform mesopores such as MCM-41 or SBA-15 silicate materials. Monomodal pore size distribution was observed with a broad peak at the maximum at mesopore diameter in the region of ≈ 15 nm. Due to the presence of mesopores, the specific surface area was developed ($\approx 147.16 \text{ m}^2 \text{ g}^{-1}$). The adsorption isotherms exhibited the best fit with the Freundlich adsorption isotherm and the approximation of results indicated the physisorption process on a heterogeneous surface.

Kinetics of Ammonia Adsorption

Investigation of adsorption kinetics provides information on possible adsorption mechanisms essential for the formation of the mathematical model on the process consequently revealing possible process dynamics that could be applied to the adsorbent development at an industrial level. The non-linear regression and linear regression of the pseudo-first order (PFO) adsorption kinetic model for the adsorbent CR-100 are presented in Figure 1. The kinetic results showed that the most intense

adsorption occurred in the first 30 minutes of the process where 85 % of removal was observed (Figure 1). The remaining amount of ammonia was gradually removed until the equilibrium was reached in the time interval between 100 and 120 minutes. This kinetic investigation of ammonia adsorption on the adsorbent confirmed this adsorption behaviour.^[33] The equilibrium did not occur immediately, which can be directly related to adsorbents with developed porous structure. The mass transfer from the solution to adsorption sites on adsorbent particles was limited by the mass transfer resistance which determined the time required to reach the equilibrium.^[34]

According to the non-linear PFO kinetic model (Figure 1a, Table 2), the adsorption complex is formed by the interaction of one adsorbate species with one active adsorption centre. For the linear PFO model the results (Figure 1b, Table 2) the correlation coefficient of the linear model, r , ranged from -0.936 to -0.979 , while the coefficients of determination, R^2 , ranged from 0.876 to 0.959. The calculated values of the equilibrium amount of adsorbed ammonia gave the estimated value that was twice lower than the experimental, leading to the conclusion that this model was not adequate to describe the kinetics of ammonia adsorption on the investigated mesoporous aluminosilicate adsorbent. On the contrary, in the case of non-linear PFO model the results are presented in the Table 2. The coefficients of determination, R^2 , ranged from 0.979 to 0.987. The calculated values of the equilibrium amount of adsorbed ammonia gave the estimated values that are in better agreement with the experimental results compared to the linear PFO model.

The estimated values of linear PSO model constants are presented in Table 2, Figure 2b.

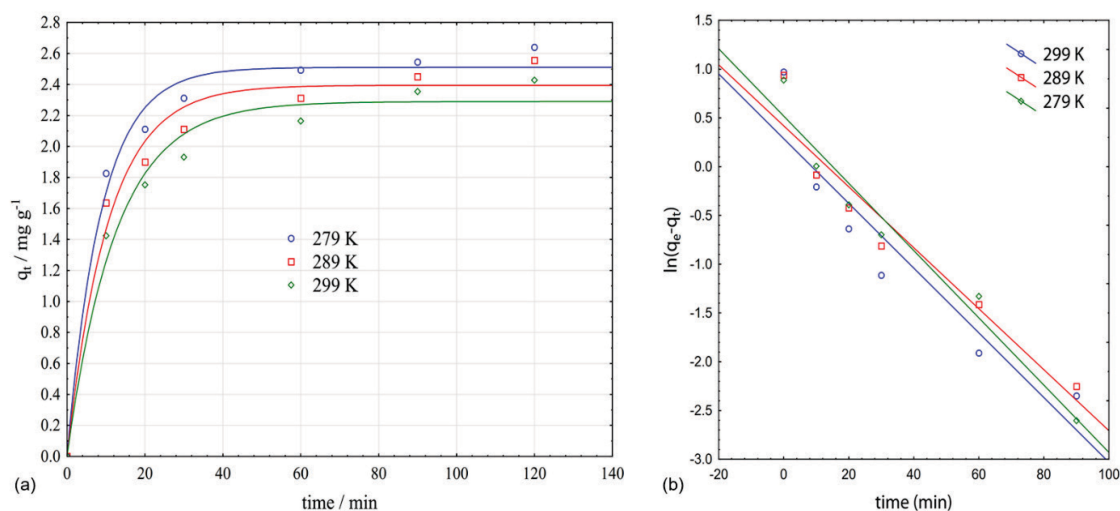


Figure 1. Pseudo-first order (PFO) adsorption kinetic model for the adsorbent CR-100: (a) non-linear regression (b) Linear regression kinetic model.

Table 2. Calculated parameters of non-linear and linear PFO and PSO kinetic models for ammonia adsorption by CR-100 adsorbent.

Non-linear regression pseudo first-order kinetic model						
<i>T</i> / K	<i>q_{e,exp}</i> / mg g ⁻¹	<i>q_{e,model}</i> / mg g ⁻¹	<i>k</i> ₁ / min ⁻¹	<i>R</i> ² / -		
279	2.429	2.510	0.113	0.987		
289	2.555	2.395	0.095	0.978		
299	2.640	2.289	0.080	0.979		
Linear regression pseudo first-order kinetic model						
<i>T</i> / K	<i>q_{e,exp}</i> / mg g ⁻¹	<i>q_{e,model}</i> / mg g ⁻¹	<i>k</i> ₁ / min ⁻¹	<i>r</i> / -	<i>R</i> ² / -	
279	2.429	1.331	0.033	-0.936	0.876	
289	2.555	1.520	0.031	-0.961	0.924	
299	2.640	1.680	0.035	-0.979	0.959	
Non-linear regression pseudo second-order kinetic model						
<i>T</i> / K	<i>q_{e,exp}</i> / mg g ⁻¹	<i>q_{e,model}</i> / mg g ⁻¹	<i>k</i> ₂ / g min ⁻¹ mg ⁻¹	<i>R</i> ² / -	<i>h</i> / mg g ⁻¹ min ⁻¹	
279	2.429	2.710	0.072	0.999	0.529	
289	2.555	2.626	0.056	0.996	0.386	
299	2.640	2.548	0.045	0.997	0.292	
Linear regression pseudo second-order kinetic model						
<i>T</i> / K	<i>q_{e,exp}</i> / mg g ⁻¹	<i>q_{e,model}</i> / mg g ⁻¹	<i>k</i> ₂ / g min ⁻¹ mg ⁻¹	<i>r</i> / -	<i>R</i> ² / -	<i>h</i> / mg g ⁻¹ min ⁻¹
279	2.429	2.608	0.039	0.999	0.999	0.263
289	2.555	2.695	0.046	0.999	0.999	0.332
299	2.640	2.742	0.064	0.999	0.999	0.482

The correlation and determination coefficients have high values for all three observed temperatures. The equilibrium amounts of adsorbed ammonia estimated by the pseudo second-order model were higher than the

experimental values at the observed temperatures (7.4 % higher *q_e* at 279 K, 5.5 % at 289 K and 3.9 % at 299 K). In addition to the good equilibrium concentration estimates, an increasing trend of model parameters values and

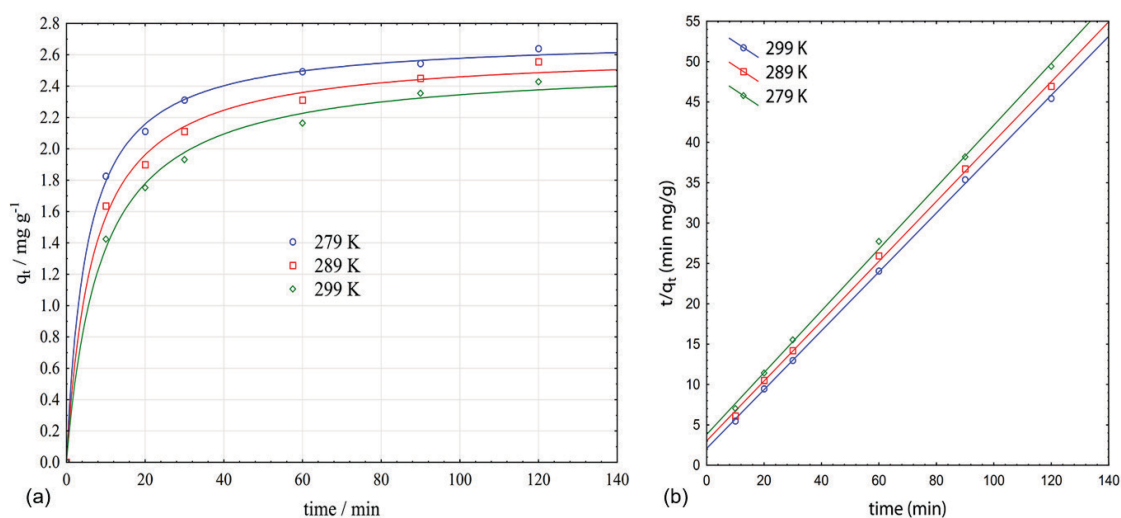


Figure 2. Pseudo- second order (PSO) adsorption kinetic model for the adsorbent CR-100: (a) non-linear regression (b) Linear regression kinetic model.

reaction rate constants was observed with the increase of the temperature, indicating the endothermic character of the removal process on the investigated adsorbent CR-100. These results suggest that the complex adsorption/ion exchange processes occur.

The results of non-linear PSO regression kinetic model are presented in Figure 2a and Table 2.

The same trend was also observed for initial adsorption rate. Considering ammonia concentrations at the beginning of adsorption ($\sim 2.3 \text{ mg L}^{-1}$), the high adsorption rates could be explained by high availability of the active sites, as well as by high ammonia concentration during the first 30 minutes of the process, followed by a gradual approach to the equilibrium.^[33]

From the parameters presented in Table 2 it can be observed that the determination coefficients for the non-linear PSO have higher values for all three studied temperatures compared to the non-linear PFO kinetic model. The equilibrium amounts of adsorbed ammonia estimated by the non-linear pseudo second-order model were higher than the experimental values for 279 K and 289 K, while at the highest temperature (299 K) the value is slightly lower. On the other hand, results suggest that the complex adsorption/ion exchange processes occurred indicated by the decreasing trend of reaction rate constants with the increase of the temperature.

For additional determination of adsorption kinetics, the Elovich model was used. This model is based on adsorption capacity, with the assumption that the adsorbent solid surface is energetically heterogeneous and that adsorption kinetics at low surface coverage is not influenced by desorption and interactions between the adsorbed species. Furthermore, the model also includes the assumption that the adsorption rate decreases exponentially with the increase of the adsorbed amount.^[35]

The results of the data fitting with the non-linearized and linearized Elovich model are presented in Table 3 and Figure 3. The linearized form of the Elovich model (Figure 3b. Table 3) had high values of the correlation coefficient for all three temperatures. The initial adsorption rate, α , decreased with the increasing temperature, while the desorption coefficient, β , increased. These results indicated a decrease in the chemisorption rate with the increase of the temperature, although such high values of the initial rate significantly deviated from the values obtained for the pseudo second-order model. The explanation for these results could be in the calculation method for the initial adsorption rate, α , that was obtained from the calculated data for the desorption coefficient. The non-linear Elovich model had slightly higher values of the determination coefficient for all three temperatures compared to the linear form (Figure 3a. Table 3). In contrast to the linear

Table 3. Calculated parameters for the non-linear and linear Elovich kinetic model.

T/K	Non-linear Elovich kinetic model			Linear Elovich kinetic model			
	$\alpha/\text{mg g}^{-1}\text{min}^{-1}$	$\beta/\text{mg g}^{-1}$	$R^2/-$	$\alpha/\text{mg g}^{-1}\text{min}^{-1}$	$\beta/\text{mg g}^{-1}$	$r/-$	$R^2/-$
279	11.811	3.143	0.997	117.281	0.318	0.985	0.971
289	3.302	2.721	0.999	25.132	0.985	0.997	0.994
299	1.432	2.465	0.999	9.239	0.971	0.997	0.995

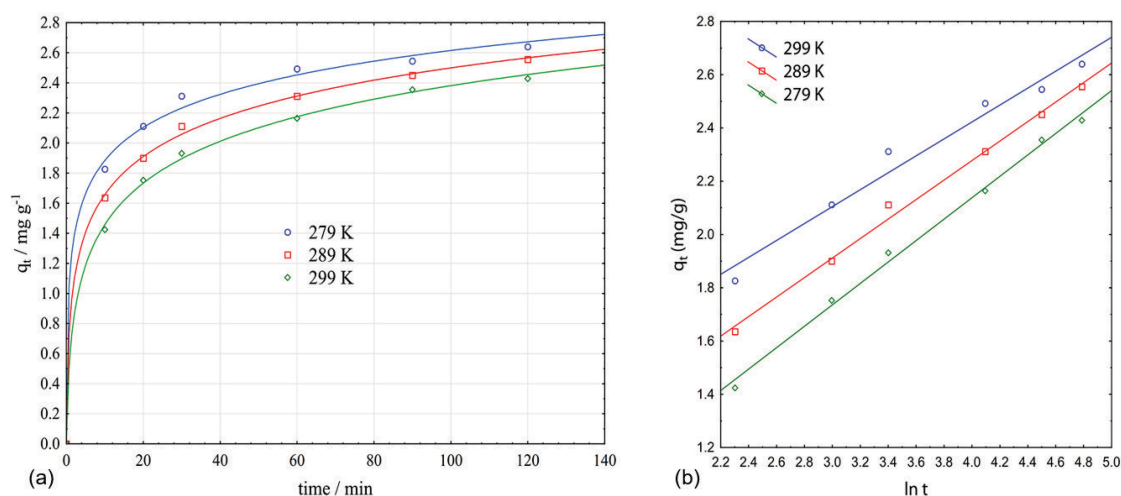


Figure 3. The non-linear (a) and linear (b) Elovich kinetic model for the adsorbent CR-100.

form, results of the non-linear Elovich model suggests that both α and β decreased with the with the increasing temperature. At the same time calculated values of the initial rate are smaller compared to values obtained from the linear regression. These results confirmed chemisorption nature of adsorption.

Further analysis of the adsorption process mechanism was conducted by applying the liquid film diffusion model (LFD) and presented in Figure 4 and Table 4. For the mechanism determination in both cases the initial (0,0) point was excluded from analysis and only linear regression was used. Furthermore, the non-linear IPD regression model exhibited positive intercept with the ordinate (*i.e.* $C > 0$) indicating that some adsorbate amount was already adsorbed at the initial point at $t = 0$ which is not physically possible and therefore only the linear regression was used.^[32] LFD is based on the equation of mass transfer rate through a liquid film that is formed around the adsorbent particles. The liquid film diffusion model correlation linear coefficient values were in the range from -0.894 to -0.935 (Table 4, Figure 4). Such values indicated a significant linear relationship between the observed variables.

However, the values of the determination coefficient were lower and ranged from 0.799 to 0.874. The model of ion diffusion kinetics through the film to the particle surface greatly affected the overall mass transfer rate, especially during the initial 30 minutes of the process. It is important to emphasize that this phase had a particularly pronounced impact when it comes to heterogeneous surfaces, as is the case with mesoporous adsorbents. For this reason, the model was fitted only for the period of the first 30 minutes of the ammonia adsorption process, Table 4. The obtained results for the period of the first 30 minutes exhibited better approximation for the liquid film diffusion model. This behaviour could have been expected since the diffusion of ions from the solution to the film formed around the adsorbent particles had no impact when the suspension was stirred, thus preventing the occurrence of concentration gradient.

Although this model obtained a high degree of correlation with the experimental data, the slopes describing the kinetics did not pass through the origin, indicating that the ammonia diffusion through the film on the particle surface was not the only mechanism controlling

Table 4. Calculated parameters for liquid film diffusion model for the complete process and for the first 30 minutes of the process.

T/K	Complete process				First 30 minutes of the process			
	Intercept / -	k_{fd} / min^{-1}	$r / -$	$R^2 / -$	Intercept / -	k_{fd} / min^{-1}	$r / -$	$R^2 / -$
279	0.360	0.003	-0.935	0.873	0.508	0.009	-0.986	0.972
289	0.317	0.003	-0.935	0.874	0.450	0.009	-0.998	0.996
299	0.253	0.002	-0.894	0.799	0.395	0.010	-0.995	0.990

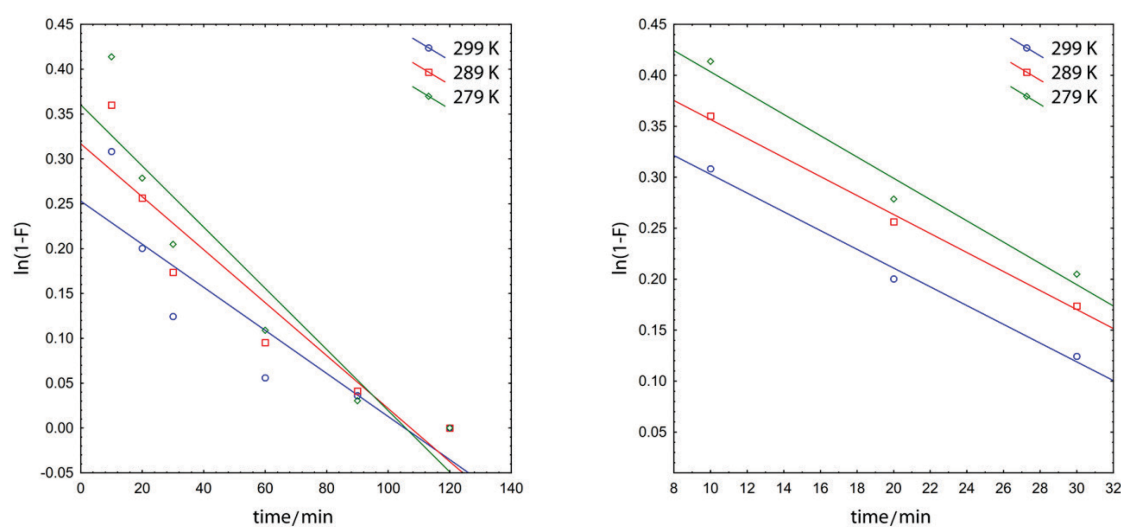


Figure 4. The liquid film diffusion model for the complete adsorption process (left) and for the first 30 minutes of the adsorption process (right).

the total adsorption rate for the adsorbent CR-100. Therefore, the applicability of the liquid film diffusion model in the present adsorption system is limited. The effect of the liquid film was observed in the first 30 minutes of adsorption when the process on the surface was rapid, since there was a large number of available, active centres on the adsorbent surface.^[36]

If the diffusion of adsorbate particles through the adsorbent is the limiting step of the adsorption rate, the intra-particle diffusion model (IPD) or the Weber-Morris model should be considered (Table 5, Figure 5). The IPD correlation coefficient was in the range from 0.947 to 0.975. Such values of the linear correlation coefficient indicated a significant linear relationship between the observed parameters. However, the values of the determination coefficient had lower values ranging from 0.896 to 0.951. It can be concluded that this model can partially be applied to the investigated system. The linear dependence ($q_t - t^{1/2}$) did not pass through the coordinate origin, leading to the conclusion that in addition to intra-particle diffusion, the external mass transfer was also the controlling step in the total adsorption rate. The positive values of intercept indicated that the boundary layer

Table 5. Calculated parameters for intra-particle diffusion model.

T/K	Intercept/-	k_f/min^{-1}	r/-	R ² /-
279	1.159	0.124	0.975	0.951
289	1.387	0.113	0.975	0.950
299	1.661	0.096	0.947	0.896

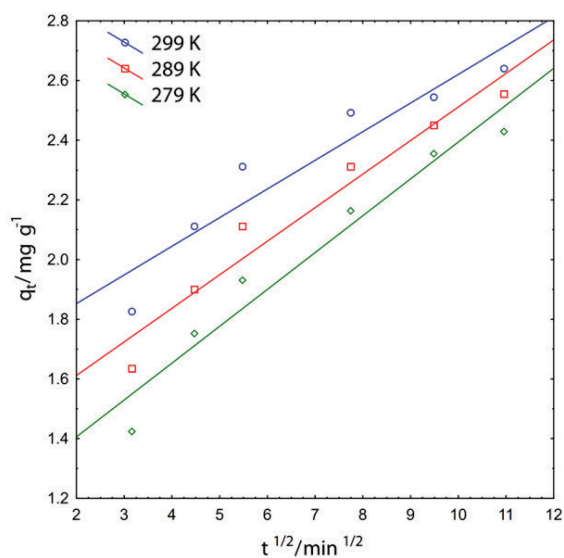


Figure 5. Intra-particle diffusion model for the adsorbent CR-100.

influenced the adsorption rate. The IPD rate constant values decreased with the temperature increase, which can be explained by higher resistance to diffusion due to the increased mobility of the dissolved species at higher temperatures and the density decrease of the aqueous solution.

Thermodynamics of Ammonia Adsorption on the Adsorbent CR-100

In order to obtain the information on the adsorption type and mechanism, as well as to gain insights into the limiting step, temperature dependence of the adsorption process was examined. Depending on the structure and type of active centres on the adsorbent surface, temperature can influence the adsorption capacity, while the thermodynamic parameters can determine the nature of the adsorption process, as well as values of enthalpy, entropy and free Gibbs energy.

Evaluation of Thermodynamic Parameters

The obtained results from the adsorption kinetics indicated that the pseudo second-order model was the best fit for the experimental results. The value of activation energy can reveal whether the process is dominant physisorption (E_a in the range 5–40 kJ mol⁻¹) or chemisorption (E_a in the range 40–800 kJ mol⁻¹)^[36] The parameters calculated from the Arrhenius equation (Eq. 8) were as follows: activation energy was 17.496 kJ mol⁻¹, Arrhenius pre-exponential factor was 1.449, linear correlation coefficient was -0.978 and, the coefficient of determination was 0.957 (Figure 6). The obtained activation energy values point out that physisorption was predominant the adsorption type. Also, low values of the activation energy explained the high process rate.

The activation enthalpy and entropy from the Eyring's equation (Eq. 9) for the pseudo second-order

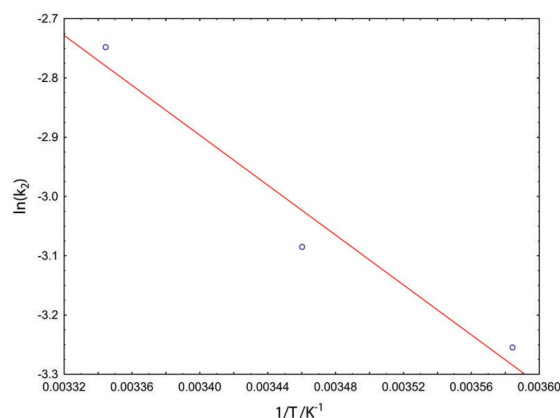


Figure 6. The Arrhenius equation for the adsorbent CR-100.

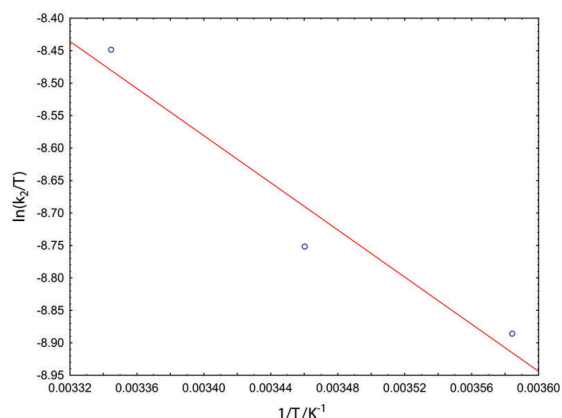


Figure 7. Eyring's equation for the adsorbent CR-100.

model was determined from the linear fit presented in Figure 7. The linear correlation coefficient was -0.972 , the coefficient of determination was 0.944 , while the activation entropy and enthalpy were $-217.543 \text{ J mol}^{-1} \text{ K}^{-1}$ and $15.096 \text{ kJ mol}^{-1}$, respectively. Negative values of activation entropy suggested the associative adsorption of ammonia on the mesoporous adsorbent surface, indicating the presence of the interaction between the adsorbed molecules. Positive values of the activation enthalpy indicated that it was a complex adsorption/ion exchange endothermic removal process, which was confirmed by the data obtained from the equilibrium concentrations at different temperatures. From the values of activation enthalpy and entropy, the free Gibbs activation energy was determined: $80.278 \text{ kJ mol}^{-1}$, $78.098 \text{ kJ mol}^{-1}$ and $75.918 \text{ kJ mol}^{-1}$, for temperatures of 299 K , 288 K and 279 K , respectively. These high and positive values of free activation energy indicated that the energy was essential for the removal process, as reported in the literature.^[36]

A comparison of Arrhenius and Eyring's equations revealed that there is analogy between the activation energy and the activation enthalpy, as well as between the Arrhenius pre-exponential factor, $\ln A$, and the activation entropy. Low values of the activation energy and enthalpy occurred at high process velocities, so a high adsorption rate can be expected, which is in accordance with the experimentally obtained results.

Equilibrium Thermodynamic Parameters

The change in the standard free Gibbs energy, ΔG , (Eqs. 10 and 11) was used to determine the spontaneity of the adsorption process, knowing that negative values of the ΔG indicate a spontaneous process. The results of the calculated thermodynamic data are shown in Table 6.

The ammonia adsorption from the observed solution was a spontaneous process, since all free energy values were negative. Values of ΔG up to -20 kJ mol^{-1} suggest

Table 6. Thermodynamic parameters of ammonia adsorption.

T/K	$K_b/\text{mg L}^{-1}$	K_c	$\Delta G/\text{kJ mol}^{-1}$	$\Delta H/\text{kJ mol}^{-1}$	$\Delta S/\text{kJ mol}^{-1}$
$R^2 = 0,999$					
279	1.6197	1619.7	-17.144		
289	2.0096	2009.6	-18.277	13.990	0.112
299	2.4242	2424.2	-19.376		

physical adsorption occurring as a result of electrostatic interaction between the binding sites and adsorbate, whereas values less than -40 kJ mol^{-1} , indicate chemisorption including adsorbate-adsorbent electron exchange with the formation of chemical bonds. The calculated ΔG values (Table 6) indicated the physisorption of ammonia on the adsorbent surface. The obtained positive enthalpy values indicated that the process was endothermic, which was reflected in the increased ammonia removal with increasing temperature. Small, positive entropy values also confirmed physical adsorption. Positive entropy values additionally corroborated the spontaneity of adsorption process.

Isosteric Adsorption Heat

The type of adsorption and the characterization of the adsorbent surface was determined using data obtained from the isosteric heat (Eqs. 12 and 13). The dependence of the isosteric heat on the constant amount of adsorbed ammonia, q_e is presented in Figure 8. The change in the isosteric heat revealed a typical dependence for energy heterogeneous adsorbent surfaces validating the results obtained from the Freundlich adsorption isotherm.

Low values of the constant adsorbed ammonia amount and small coverage of the surface with the adsorbent indicate chemisorption with the values of isosteric heat around 24 kJ mol^{-1} . Most likely, at the beginning of the adsorption process ammonia bonded to the most energy-rich active sites, that could probably be linked to ion exchange occurrence. Further increase of the surface coverage leads to a decrease in the isosteric heat, which unequivocally indicates the energy heterogeneity of the adsorbent surface.

The change in isosteric heat shown in Figure 8 can be divided into two separate regions. In the first region, the values decrease quite steeply until the constant equilibrium amount of adsorbed ammonia reached a value of about 8 to 9 mg g^{-1} . The further decrease in the value of the isosteric heat was much milder and the value had an approximately constant value between 14 and 15 kJ mol^{-1} . This phenomenon can be explained by the action of two mutually opposite effects during the process of ammonia adsorption on the surface of adsorbent CR-100. Namely, adsorption initially occurred on active sites with the highest

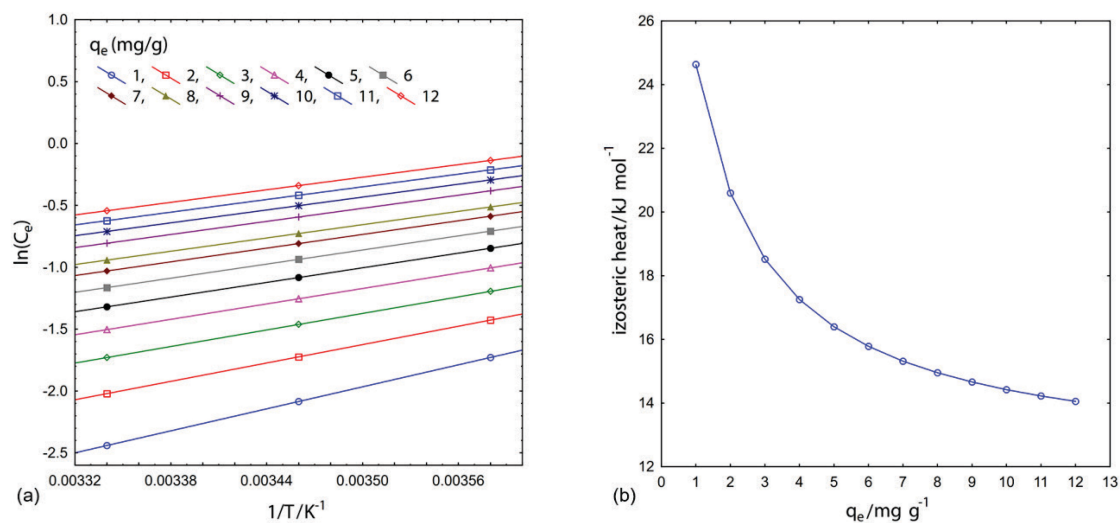


Figure 8. Isothermic heat: (a) dependence of $\ln(C_e)$ as a function $1/T$, (b) isothermic heat as a function of a constant amount of adsorbed ammonia.

energy, resulting in a declining trend of the isothermic heat value with the increase of surface coverage. However, as the amount of adsorbed ammonia on the adsorbent surface increased, there were lateral interactions and establishment of bonds between the adsorbed molecules on the adsorbent surface. Therefore, the larger the number of adsorbed molecules on the surface, the contribution of lateral heat adsorption interactions increased.^[38] These two effects, which in opposite ways affected the values of the isothermal adsorption heat, mutually compensated their actions. This compensatory effect occurred at certain level of coverage of the adsorption surface and at certain amount of adsorbed ammonia molecules. This phenomenon occurred in the second part of the isothermic heat change, when the change in the isothermic heat value is lower and can be observed as a approximately constant value.

CONCLUSION

The study shows that the synthetic adsorbent Crystal-Right™ (CR-100) can be used as an adsorbent for ammonia removal from aqueous solution. It was concluded that several factors influenced the adsorption properties of adsorbent CR-100 in aqueous solution. The Freundlich isotherm model showed the best fit to the equilibrium adsorption data for all temperatures. The adsorption data revealed good agreement with the pseudo-second-order kinetic model where the correlation and determination coefficients had high values for all three observed temperatures. The rate constant increased with increase in temperature indicating endothermic nature of ammonia removal process. From the Elovich model it was detected that chemisorption rate decreased with the temperature

increase, whereas liquid film diffusion model disclosed that overall mass transfer rate (especially in the initial 30 minutes) had evident impact on the surface energy of the mesoporous adsorbent. Furthermore, for the IPD model the linear dependence ($q_t - t^{1/2}$) did not pass through the coordinate origin, leading to the conclusion that in addition to intra-particle diffusion, the external mass transfer was also the controlling step in the total adsorption rate. The Arrhenius and Eyring equations were used to obtain the activation parameters (E_a , ΔH , ΔS and ΔG) for the adsorption system and suggested spontaneous and endothermic nature of complex adsorption/ion exchange removal process. The isothermic heat values of adsorption were calculated using the Clausius–Clapeyron equation. The isothermic heat of adsorption revealed that with the increase in surface loading lateral interactions between the adsorbed molecules occurred. Additionally, further increase of the adsorbent surface coverage leads to a decrease in the isothermic heat, which unequivocally indicates the energy heterogeneity of the adsorbent surface.

Acknowledgment. The financial support from the Provincial Secretariat for Higher Education and Scientific Research (Contract No. 142-451-2341/2021-01/02) and The Ministry of Education, Science and Technological Development of the Republic of Serbia for the investigation (Contract No. 451-03-9/2021-14/200134) is gratefully acknowledged.

Supplementary Information. Supporting information to the paper is attached to the electronic version of the article at: <https://doi.org/10.5562/cca3864>.

PDF files with attached documents are best viewed with Adobe Acrobat Reader which is free and can be downloaded from [Adobe's web site](https://www.adobe.com/acrobat).

REFERENCES

- [1] S. Mrazovac, M. Vojinović-Miloradov, I. Matić, N. Marić, *Chemie der Erde* **2013**, *73*, 217–225. <https://doi.org/10.1016/j.chemer.2012.11.002>
- [2] N. Marić, S. Mrazovac Kurilić, I. Matić, S. Sorajčić, J. Zarić, *Environ. Earth Sci.* **2014**, *72*, 525–534. <https://doi.org/10.1007/s12665-013-2973-z>
- [3] G. Devic, D. Djordjevic, S. Sakan, *Sci. Total. Environ.* **2014**, *468–469*, 933–942. <https://doi.org/10.1016/j.scitotenv.2013.09.011>
- [4] V. K. Gupta, H. Sadegh, M. Yari, G. R. Shahryari, B. Maazinejad, M. Chahardori, *Glob. J. Environ. Sci. Manag.* **2015**, *1*, 149–158.
- [5] J. Huang, N. R. Kankanamge, C. Chow, D. T. Welsh, T. Li, P. R. Teasdale, *J Environ. Sci. (China)* **2018**, *63*, 174–197. <https://doi.org/10.1016/j.jes.2017.09.009>
- [6] Y. Zheng, Y. Liu, A. Wang, *Chem. Eng. J.* **2011**, *171*, 1201–1208. <https://doi.org/10.1016/j.cej.2011.05.026>
- [7] H. Kurama, J. Poetzschke, R. Haseneder, *Water Res.* **2002**, *36*, 2905–2909. [https://doi.org/10.1016/S0043-1354\(01\)00531-0](https://doi.org/10.1016/S0043-1354(01)00531-0)
- [8] R. R. Karri, J. N. Sahu, V. Chimmiri, *J. Mol. Liq.* **2018**, *261*, 21–31. <https://doi.org/10.1016/j.molliq.2018.03.120>
- [9] Ž. Tomić, M. Kukučka, N. K. Stojanović, A. Kukučka, A. Jokić, *J. Environ. Sci. Heal - Part A Toxic/Hazardous Subst. Environ. Eng.* **2016**, *51*, 1068–1074. <https://doi.org/10.1080/10934529.2016.1198629>
- [10] D. Drljača, S. Maletić, B. Dalmacija, *Hem. Ind.* **2019**, *73*, 249–264. <https://doi.org/10.2298/HEMIND190211022D>
- [11] B. Han, C. Butterly, W. Zhang, J. He Zheng, D. Chen, *J. Clean Prod.* **2021**, *283*, 124611. <https://doi.org/10.1016/j.jclepro.2020.124611>
- [12] M. Shaban, M.R. AbuKhadra, F. M. Nasief, H. M. Abd El-Salam, *Water Air Soil Pollut.* **2017**, *228*, 450. <https://doi.org/10.1007/s11270-017-3643-7>
- [13] K. Margeta, N. Z. Logar, M. Šiljeg, A. Farkas, in *Water Treatment* (Eds.: W. Elshorbagy, R. K. Chowdhury), IntechOpen, **2013**. <https://doi.org/10.5772/50738>
- [14] M. Voccianta, A. De Folly D'Auris, A. Finocchi, M. Tagliabue, M. Bellettato, A. Ferrucci, A. P. Reverberi, S. Ferro, *J Clean Prod.* **2018**, *198*, 480–487. <https://doi.org/10.1016/j.jclepro.2018.07.025>
- [15] A. Langella, M. Pansini, P. Cappelletti, B. De Gennaro, M. De' Gennaro, C. Colella, *Microporous Mesoporous Mater.* **2000**, *37*, 337–343. [https://doi.org/10.1016/S1387-1811\(99\)00276-0](https://doi.org/10.1016/S1387-1811(99)00276-0)
- [16] A. Demir, A. Günay, E. Debik, *Water SA.* **2002**, *28*, 329–336. <https://doi.org/10.4314/wsa.v28i3.4903>
- [17] Y. Wang, F. Lin, W. Pang, *J Hazard Mater.* **2008**, *160*, 371–375. <https://doi.org/10.1016/j.jhazmat.2008.03.006>
- [18] M. Delkash, B. Ebrazi Bakhshayesh, H. Kazemian, *Microporous Mesoporous Mater.* **2015**, *214*, 224–241. <https://doi.org/10.1016/j.micromeso.2015.04.039>
- [19] P. Misaelides, *Microporous Mesoporous Mater.* **2011**, *144*, 15–18. <https://doi.org/10.1016/j.micromeso.2011.03.024>
- [20] H. S. Sherry, *J. Phys. Chem.* **1966**, *70*, 1158–1168. <https://doi.org/10.1021/j100876a031>
- [21] H. S. Sherry, *J. Phys. Chem.* **1968**, *72*, 4086–4094. <https://doi.org/10.1021/j100858a024>
- [22] I. Petrov, T. Michalev, Proceedings of the University of Ruse “Angel Kanchev” **2012**, *51*, 30–35.
- [23] H. Ghobarkar, U. Guth, *Prog. Solid. State Ch.* **1999**, *27*, 29–73. [https://doi.org/10.1016/S0079-6786\(00\)00002-9](https://doi.org/10.1016/S0079-6786(00)00002-9)
- [24] M. Li, X. Zhu, F. Zhu, G. Ren, G. Cao, L. Song, *Des.* **2011**, *271*, 295–300. [https://doi.org/10.1016/S0079-6786\(00\)00002-9](https://doi.org/10.1016/S0079-6786(00)00002-9)
- [25] X. Meng, F-S. Xiao, *Chem Rev.* **2014**, *114*, 1521–1543. <https://doi.org/10.1021/cr4001513>
- [26] X. Y. Li, Y. Jiang, X. Q. Liu, L. Y. Shi, D. Y. Zhang, L. B. Sun, *ACS Sustain. Chem. Eng.* **2017**, *5*, 6124–6130. <https://doi.org/10.1021/acssuschemeng.7b01001>
- [27] S. Wang, Y. Peng, *Chem. Eng. J.* **2010**, *156*, 11–24. <https://doi.org/10.1016/j.cej.2009.10.029>
- [28] Y. Liu, C. Yan, J. Zhao, Z. Zhang, H. Wang, S. Zhou, L. Wu, *J. Clean Prod.* **2018**, *202*, 11–22. <https://doi.org/10.1016/j.jclepro.2018.08.128>
- [29] L. Lazar, B. Bandrabur, R.E. Tataru-Fărnuș, M. Drobotă, S. G. Stroe, G. Gutt, *Environ. Eng. Manag. J.* **2015**, *14*, 541–549. <https://doi.org/10.30638/eemj.2015.058>
- [30] I. Skoczko, J. Piekutin, K. Ignatowicz, *Desalin Water Treat.* **2016**, *57*, 1611–1619. <https://doi.org/10.1080/19443994.2015.1043487>
- [31] Ž. Tomić, Mogućnost primene sintetičkog zeolita CR-100 (Crystal-Right™) za adsorpciju amonijaka iz podzemnih voda Banatskog akvifera. PhD Thesis, Faculty of Technology Novi Sad, University of Novi Sad, **2016**.
- [32] B. Obradovic, *Hem Ind.* **2020**, *74*, 65–70. <https://doi.org/10.2298/HEMIND200201006O>
- [33] F. Mazloomi, M. Jalali, *J. Environ. Chem. Eng.* **2016**, *4*, 240–249. <https://doi.org/10.1016/j.jece.2015.11.001>
- [34] E. Worch, *Adsorption Technology in Water Treatment. Fundamentals, Processes and Modelling*. Walter de Gruyter GmbH&Co. KG, Berlin/Boston; **2012**. <https://doi.org/10.1515/9783110240238>

- [35] S. Gupta Sen, K. G. Bhattacharyya, *Adv. Colloid Interface Sci.* **2011**, *162*, 39–58.
<https://doi.org/10.1016/j.cis.2010.12.004>
- [36] S. Chowdhury, R. Mishra, P. Saha, P. Kushwaha, *Desalination.* **2011**, *265*, 159–168.
<https://doi.org/10.1016/j.desal.2010.07.047>
- [37] S. K. Milonjić, *J. Serbian Chem. Soc.* **2007**, *72*, 1363–1367.
<https://doi.org/10.2298/JSC0712363M>
- [38] H. E. Eguez, E. H. Cho, *Jom.* **1987**, *39*, 38–41.
<https://doi.org/10.1007/BF03258040>